

# Age constraints for rocks hosting massive sulphide mineralization at Rock and Roll and Granduc deposits between Iskut and Stewart, British Columbia



Mitchell G. Mihalynuk<sup>1, a</sup>, Alexandre Zagorevski<sup>2</sup>, James M. Logan<sup>3</sup>, Richard M. Friedman<sup>4</sup>, and Stephen T. Johnston<sup>5</sup>

<sup>1</sup> British Columbia Geological Survey, Ministry of Energy, Mines and Petroleum Resources, Victoria, BC, V8W 9N3

<sup>2</sup> Geological Survey of Canada, Ottawa, ON, K1A 0E8

<sup>3</sup> JLoGeologic, Victoria, BC, V8L 5Z9

<sup>4</sup> Pacific Centre for Isotopic and Geochemical Research, The University of British Columbia, Vancouver, BC, V6T 1Z4

<sup>5</sup> Earth & Atmospheric Science, University of Alberta, Edmonton, AB, T6G 2E1

<sup>a</sup> corresponding author: Mitch.Mihalynuk@gov.bc.ca

Recommended citation: Mihalynuk, M.G., Zagorevski, A., Logan, J.M., Friedman, R.M., and Johnston, S.T., 2019. Age constraints for rocks hosting massive sulphide mineralization at Rock and Roll and Granduc deposits between Iskut and Stewart, British Columbia. In: Geological Fieldwork 2018, British Columbia Ministry of Energy, Mines and Petroleum Resources, British Columbia Geological Survey Paper 2019-01, pp. 97-111.

## Abstract

U-Pb geochronological results reported here for host rocks of the Rock and Roll and Granduc volcanogenic massive sulphide (VMS) deposits in the Iskut area of northwestern British Columbia are consistent with the Late Triassic age suggested by previous workers. Although a direct age determination is still lacking, we constrain mineralization to between ~222 Ma and <~208 Ma for Granduc and 292 Ma to 186 Ma for Rock and Roll. The Late Triassic age may mark an important VMS mineralizing event within the submarine Stuhini arc, with implications for regional mineral exploration. Data from this study also provides constraints on two phases of superimposed deformation to between 210 Ma and 183 Ma.

**Keywords:** Volcanogenic massive sulphide, VMS, Besshi, Rock and Roll, Iskut, Granduc, geochronology, detrital zircon, Stuhini Group, Late Triassic

## 1. Introduction

Most prominent Late Triassic-Early Jurassic mineral deposits in the Stikine terrane (Stikinia) of northwestern British Columbia are calc-alkaline and alkaline Cu-Au-Mo porphyries and porphyry-related gold veins (e.g., Logan and Mihalynuk, 2014). Paleozoic and Early Mesozoic volcanogenic massive sulphide (VMS) deposits are much less common but are economically significant. They include past-producing mines such as Tulsequah Chief (Late Mississippian; Childe, 1997), Eskay Creek (Middle Jurassic, Aalenian; Childe, 1996) and Granduc (Late Triassic; Childe, 1997). VMS deposits form as accumulations of base metals in hydrothermal fields near active submarine magmatic centers. VMS prospective environments, such as ocean ridges, and volcanic arc and back arc rifts and calderas, tend to produce clusters or belts of economic deposits (e.g., Galley et al., 2007), making identification of prospective time periods a key criterion in VMS exploration. Unfortunately, the lack of a detailed stratigraphic and geochronological framework for much of northwestern British Columbia hinders exploration away from known occurrences. In this contribution, we present new geochronological data from host rocks at the Granduc mine and the Rock and Roll VMS deposit (Figs. 1, 2).

Granduc is a Besshi-type massive sulphide Cu-Au-Ag deposit (Höy, 1991) located 40 km north-northwest of Stewart (Fig. 1).

Between 1971 and 1984 Granduc produced 190,143.7 tonnes Cu, 124 million g Ag and 2 million g Au (Johnson, 2012; MINFILE 104B021). At the Main Zone, Measured, Indicated and Inferred resources are 5.16, 6.16 and 30.52 million tonnes with grades of 1.58, 1.39, and 1.40% Cu, 0.17 g/t Au, and 13.7, 11.4 and 13.3 g/t Ag (Morrison et al., 2013). Including the North Zone, total Inferred resources are 44.6 million tonnes grading 1.43% Cu, 0.19 g/t Au, and 10.7 g/t Ag; all at a 0.8% Cu-equivalent cut-off grade (Morrison et al., 2013).

Granduc was considered to be Late Triassic based on U-Pb dating of multi-grain zircon fractions separated from crosscutting mafic dikes and intensely sheared mafic igneous rocks within the 'Mine Series' (Childe, 1997). However, the dikes are restricted to the footwall of the deposit and may not be coeval with mineralization. In addition, the relationship of the 'Mine Series' sample to mineralization is uncertain due to intense deformation.

Lead isotopic ages are not quantitative, however, they can be used as a guide to the relative age of mineralization. Lead isotope signatures from Granduc sulphide mineralization (Childe, 1997) overlap of the <sup>208</sup>Pb/<sup>204</sup>Pb cluster for the ~327 Ma Tulsequah VMS camp, but the <sup>207</sup>Pb/<sup>204</sup>Pb cluster also overlaps data from the Schaft Creek porphyry copper deposit (Logan et al., 2000), which is well constrained as Late Triassic

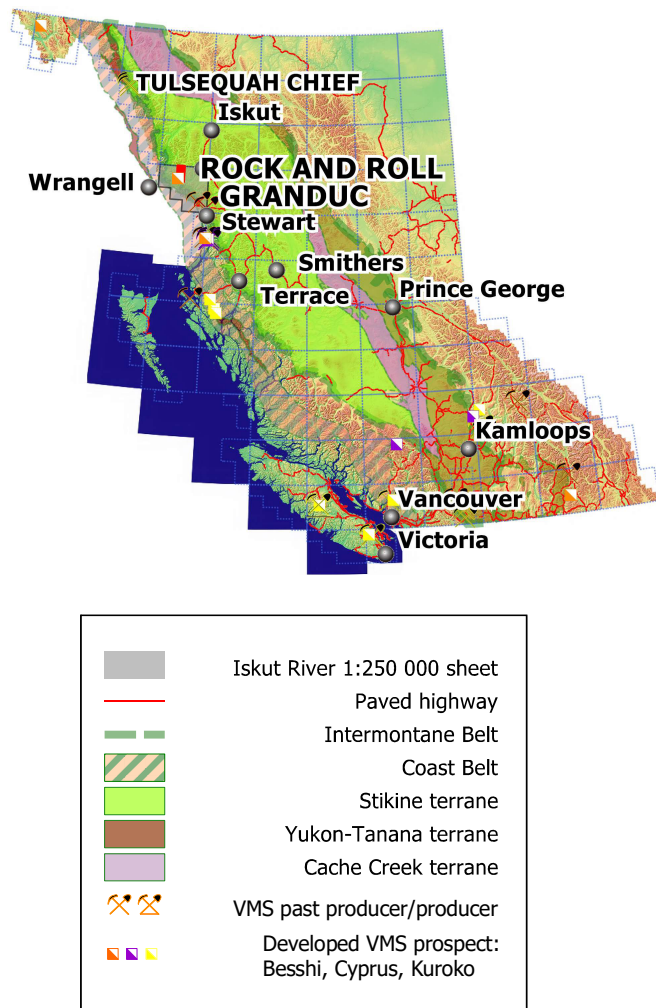


**Fig. 1.** Location of Rock and Roll and Granduc VMS deposits in northwest British Columbia. Terrane map modified after Wheeler et al. (1991).

by U-Pb dating of its host intrusive body (Scott et al., 2008). Thus, ambiguity remains as to whether Granduc lies within the Stikine assemblage (Upper Paleozoic) or the Stuhini Group (Upper Triassic).

Rock and Roll is a precious metal-rich polymetallic massive sulphide deposit (Montgomery et al., 1991) along the south side of the lower Iskut River valley (Fig. 2a), approximately 115 km northwest of Stewart. It contains an estimated Indicated resource of 2.155 million tonnes grading 0.68 g/t Au, 82.7 g/t Ag, 0.22% Cu, 0.22% Pb, and 0.94% Zn at an Au-equivalent cut-off grade of 0.5 g/t (Jones, 2011).

Geological mapping northeast of the Iskut River showed that layered rocks considered at the time to be part of the Stikine assemblage were lithologically more similar to rocks enclosing mineralization at the Rock and Roll deposit than they were to rocks of the Stuhini Group (Mihalynuk et al., 2010). However, geochronological and paleontological data to test this correlation, or to provide a direct age constraint on Rock and Roll mineralization, were lacking.

To address uncertainties regarding the age of the Granduc and Rock and Roll deposits, we collected samples of quartz-bearing clastic strata to establish maximum depositional ages using detrital zircon geochronology. In addition, we collected volcanic layers in the host stratigraphy and quartz diorite (that intrudes and shows irregular contacts with massive sulphide at Rock and Roll) for conventional CA-TIMS age determinations (Table 1). We also collected sulphide samples to determine suitability for Re-Os dating, but found these sulphides to be Re impoverished and unsuitable for dating.

## 2. Previous work and study rationale

‘Mine Series’ strata at Granduc include distinctive graphitic and tuffaceous limestone, laminated chert, mafic tuff, black argillite, heterolithic breccia (Fig. 3), and sulphides comprising 200-500 hundred metres of deformed section (Fig. 2b; Klepacki and McGuigan, unpublished map cited in McGuigan, 2005). The ~222 Ma age of the Granduc deposit is based on three U-Pb zircon age determinations that overlap within error (Childe, 1997). This age implies that Granduc is hosted by strata that are age equivalent to the Stuhini Group (Lewis, 2013), but these strata differ from the typical Stuhini Group, which is commonly characterized by augite-porphyrific volcanic rocks, polymictic conglomerate and other volcanic-derived sedimentary rocks,

**Table 1.** Synopsis of samples analyzed for geochronology and results.

Sample	Description	Longitude	Latitude	Age (Ma)	Comment
<i>Rock and Roll</i>					
TST09-3-05	Rhyolite lapilli tuff band in limestone	-131.2314	56.7143	209.7±0.9	LA-ICP-MS (data in Mihalynuk et al., 2019)
TST09-3-02	Rhyolite tuff and pyritic rhyolite tuff	-131.2323	56.7111		insufficient zircon recovery
TST09-3-16	Cherty ash tuff	-131.2251	56.7143	291.7±1.0	CA-TIMS, weighted average of 3 concordant and overlapping $^{206}\text{Pb}/^{238}\text{U}$ dates.
TST09-6-11	Diorite	-131.2315	56.7184	185.6±0.5	CA-TIMS, Maximum age of Based on $^{206}\text{Pb}/^{238}\text{U}$ date of youngest of 3 analyzed grain
TST09-7-01	Felsic dike, DDH RR-91-70, 5.2-12.2m	-131.2289	56.7188	182.9±0.2	CA-TIMS, weighted average of 4 concordant and overlapping $^{206}\text{Pb}/^{238}\text{U}$ dates.
<i>Granduc</i>					
10JLO-10-51	heterolithic breccia	-130.3505	56.1990		LA-ICP-MS (data in Mihalynuk et al., 2019)

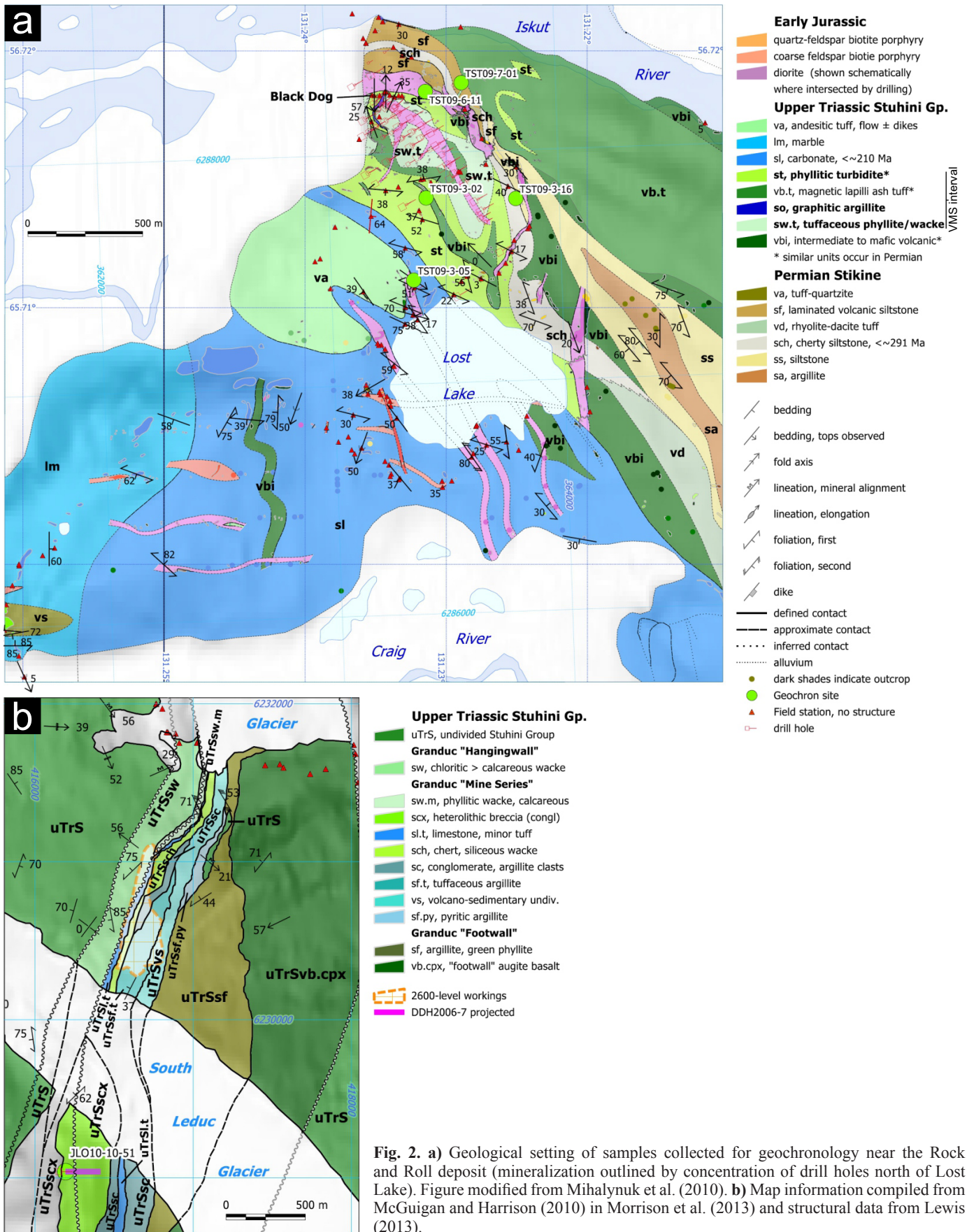
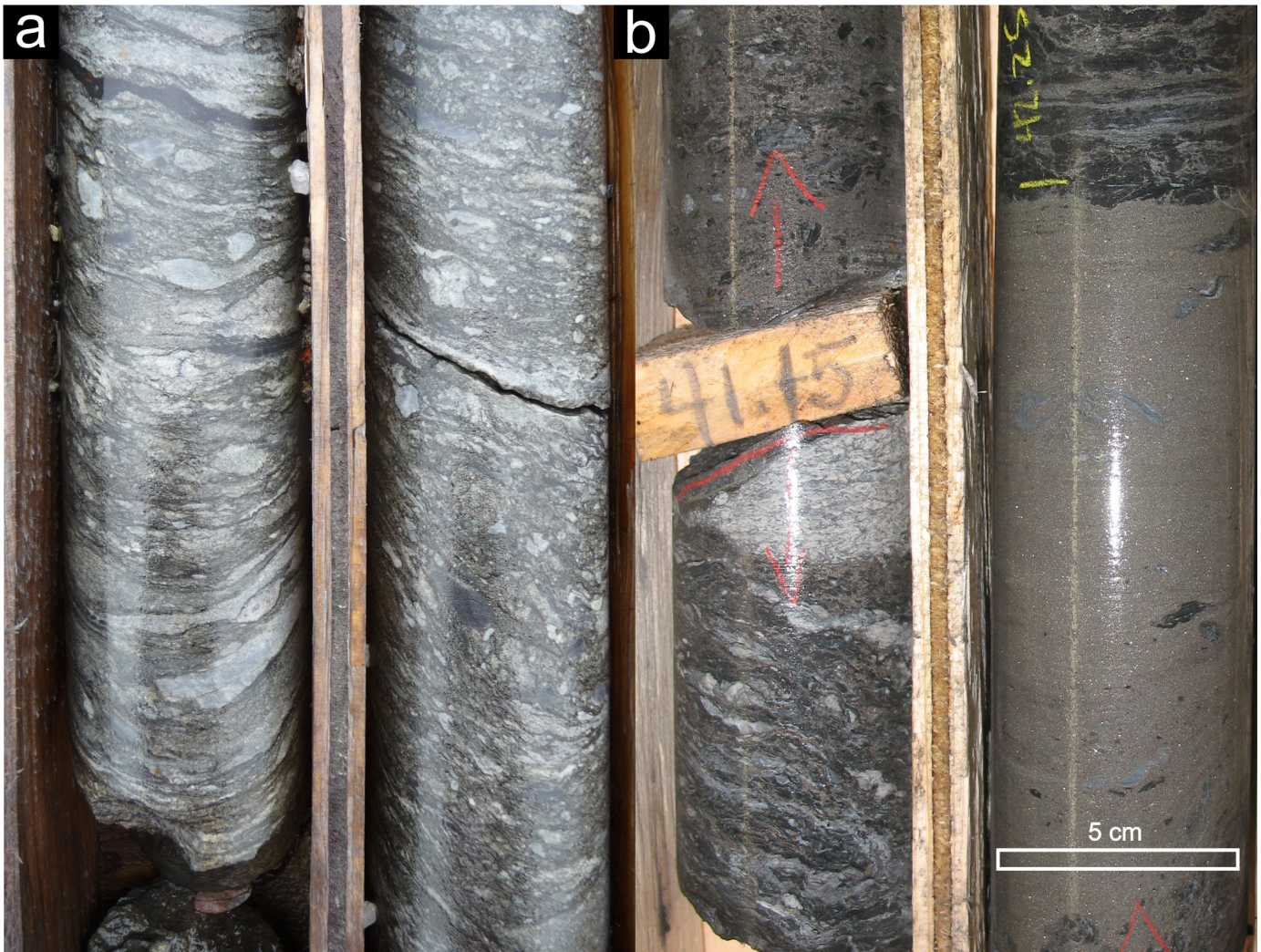


Fig. 2. a) Geological setting of samples collected for geochronology near the Rock and Roll deposit (mineralization outlined by concentration of drill holes north of Lost Lake). Figure modified from Mihalynuk et al. (2010). b) Map information compiled from McGuigan and Harrison (2010) in Morrison et al. (2013) and structural data from Lewis (2013).



**Fig. 3.** A visual comparison of mineralized foliated heterolithic breccia units. **a)** Granduc deposit drill hole 2006-7, interval submitted for detrital zircon age determination. **b)** Rock and Roll deposit drill hole RR09-107, with carbonaceous argillite (top right) and massive sulphide (mid and lower right).

and limestone. Thus, establishing a Late Triassic age for these strata is important because the Granduc Mine sequence is a distinctive succession and, if within the Stuhini Group, would be a useful regional target for VMS mineral exploration.

Re-evaluating the Granduc samples that were collected for U-Pb zircon geochronology by Childe (1997), we conclude that they are possibly all of intrusive rather than volcanic origin. A drill core sample of quartz diorite sill in the deposit footwall yielded a  $223 \pm 3$  Ma weighted mean  $^{207}\text{Pb}/^{206}\text{Pb}$  age (Childe, 1997). The second drill core sample described as “...chlorite-altered basaltic composition flow, with poorly preserved metamorphic hornblende crystals...”, also from the footwall (Childe, 1997; p. 59), yielded a  $223 \pm 5$  Ma weighted mean  $^{207}\text{Pb}/^{206}\text{Pb}$  age. Both samples produced discordant data. A third sample of “an intensely sheared rock of basaltic andesitic composition...” was collected from surface within the mineralized section. It yielded three fractions of partly resorbed (pitted and ovoid) zircons. Childe (1997) interpreted a crystallization age of  $222 \pm 1$  Ma from the concordant  $^{206}\text{Pb}/^{238}\text{U}$

ages of the three fractions. However, none of the dated samples preserve unequivocal volcanic protolith textures. All rock types sampled could be intrusive rocks that cut older strata of the succession. Therefore, we sampled strata in the immediate hangingwall of the mineralization for detrital zircons to obtain a maximum depositional age for the top of the host succession.

At the Rock and Roll prospect, previous geological investigations failed to establish the age of mineralization. Host strata are volcanogenic sedimentary rocks, sandstones, and a predominance of argillaceous to cherty strata with minor heterolithic breccia and carbonaceous argillite, which are associated with sulphide mineralization (Fig. 3). These rocks were interpreted as Triassic, overthrust by polydeformed limestone (Figs. 2a, 4) that was correlated with Paleozoic limestone elsewhere (Kerr, 1948; Mihalynuk et al., 2010). Mineralization was interpreted as stratiform (Montgomery et al., 1991). Association of stratiform mineralization with felsic volcanic rocks and high Cu-Zn (e.g., Kuroko style) suggest a syngenetic, VMS-style mineralization (Mihalynuk et al.,

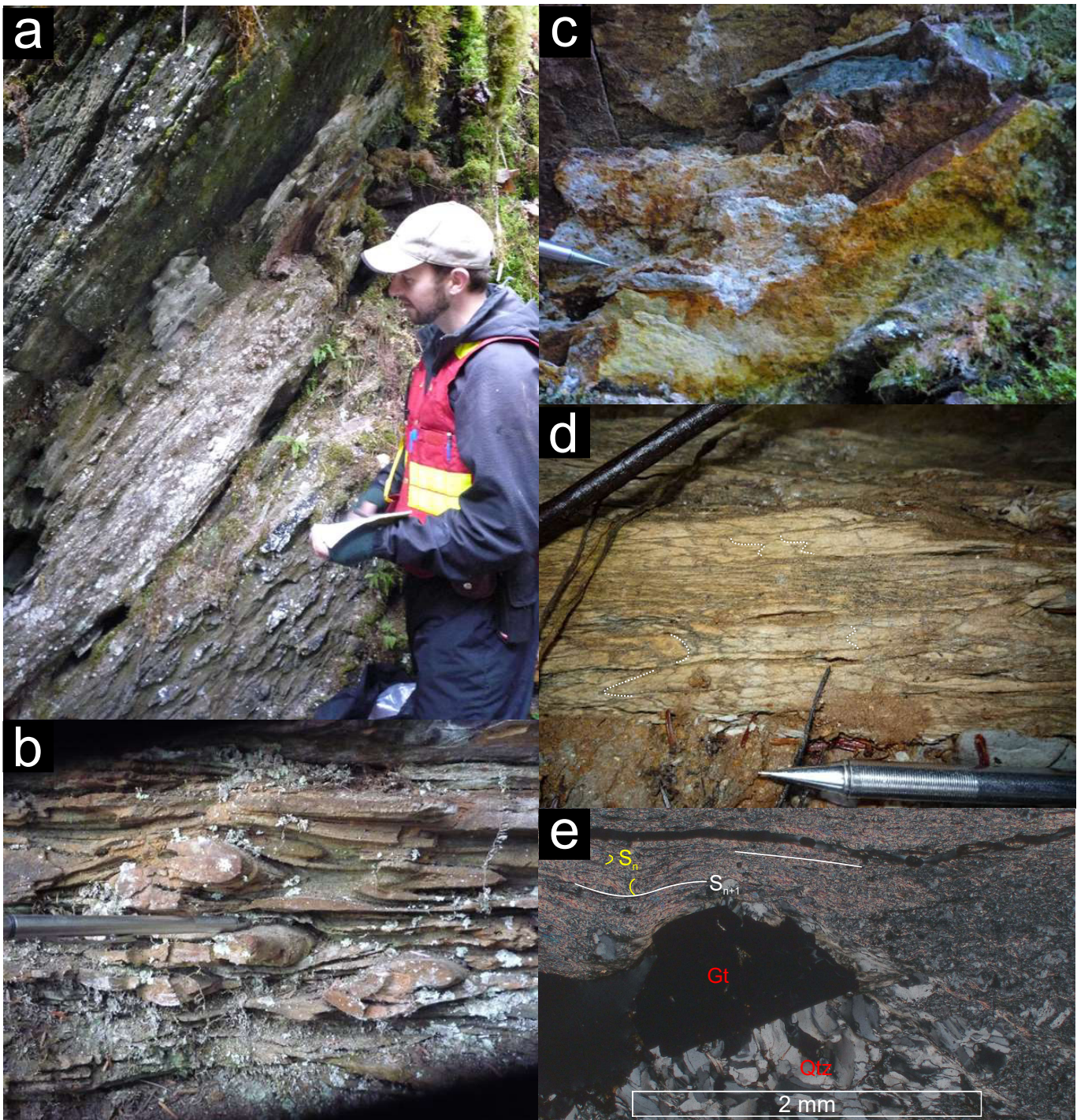


**Fig. 4.** Rock and Roll area. **a)** Outcrop of limestone with tuffaceous interbeds, like those sampled for geochronology. **b)** Limestone with isoclinal, locally rootless, folds delineated by differential weathering of resistant silty layers. Pen aligned with fold hinges. **c)** Bleached, pyritic zone of thickest tuff layer preferentially sampled for U-Pb age determination. **d)** A second phase penetrative cleavage in carbonate rocks (parallel to pen) is developed at a high angle to the earlier fabric (highlighted by dotted white curves). **e)** Photomicrograph of pyritic felsic tuff layer in limestone shows two penetrative fabrics intersecting at a high angle ( $S_n$  and  $S_{n+1}$ ). A quartz (Qtz) pressure shadow formed as the pyrite grain rotated. Iron oxide/hydroxide, possibly goethite (Gt) pseudomorphs pyrite.

2010; Foley, 1991, unpublished report cited in Jones, 2011). Mineralization is cut by diorite dikes and sills up to tens of metres thick that locally contain sulphide apophyses and enclaves remobilized from the host volcano-sedimentary rock (Fig. 5a). If Rock and Roll is a syngenetic sulphide deposit,

the age of enclosing strata should constrain the maximum age of that mineralization, whereas the age of the diorite would provide a minimum age of mineralization. We sampled both the host stratigraphy and crosscutting diorite for geochronology.

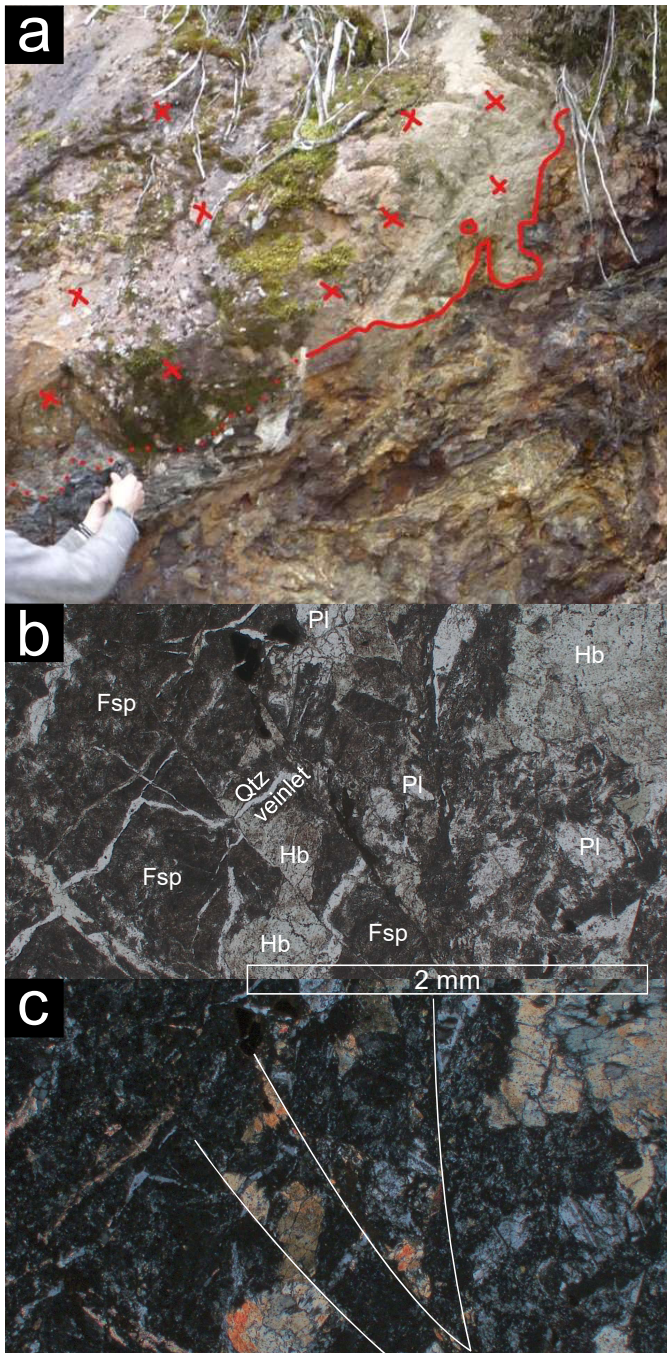


**Fig. 5. a)** Diorite cutting mineralized graphitic siltstone at the Black Dog occurrence, northwestern Rock and Roll deposit. Light-weathering massive diorite (above red line with red “x” pattern) cuts contorted, rusty, carbonaceous mudstone with massive pyrrhotite-sphalerite-chalcopyrite layers that are rusty, black orange and yellow-weathering. **b)** Plain polarized light photomicrographs of the diorite showing typically altered, turbid feldspar (Fsp) and less abundant, relatively fresh plagioclase (Pl), altered hornblende (Hb) and fine quartz veinlets (Qtz) that cut the rock along with microfaults showing variable offset. **c)** Same field of view as b) in cross polarized light; white lines highlight microfaults.

### 3. Methods

Sample preparation and analytical work for both the U-Pb Chemical Abrasion-Thermal Ionization Mass Spectrometry

(CA-TIMS) and Laser Ablation-Inductively Coupled Mass Spectroscopy (LA-ICP-MS) isotopic ages presented herein was conducted at the Pacific Centre for Isotopic and Geochemical Research (PCIGR) at the Department of Earth and Ocean Sciences, The University of British Columbia. Zircon was separated from the samples (Table 1) using standard mineral separation techniques (crushing, grinding, Wilfley wet shaker table, heavy liquids and magnetic separation), followed by hand picking. Picked samples were microscopically evaluated to ensure purity (Fig. 6a, inset). Chemically abraded single zircon grains were analyzed.

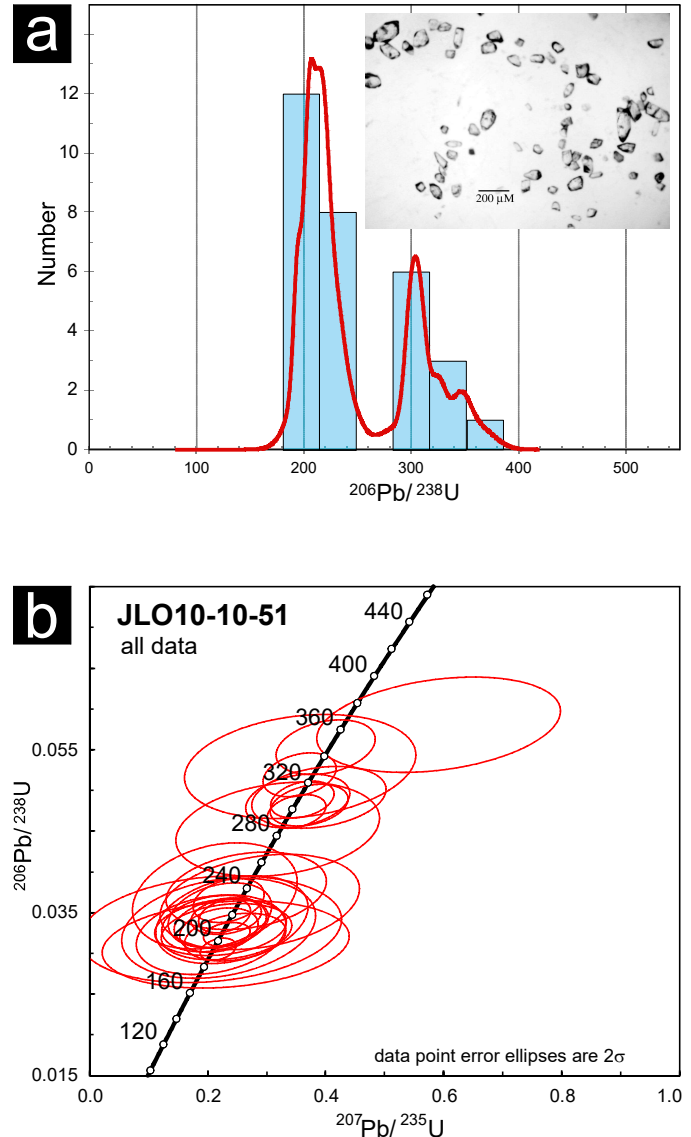


**Fig. 6. a)** Detrital zircon age histogram and distribution plot for detrital zircons obtained from heterolithic breccia within the Granduc mine stratigraphy (see Fig. 3 for sample analyzed). A representative zircon sample aliquot analyzed is shown in the inset. **b)** Concordia plot showing all of the analytical results with  $2\sigma$  error envelopes.

### 3.1. CA-TIMS

CA-TIMS procedures described here are modified from Mundil et al. (2004), Mattinson (2005), and Scoates and Friedman (2008). After rock samples underwent standard mineral separation procedures, zircons were handpicked in alcohol. The clearest, crack- and inclusion-free grains were selected, photographed and then annealed in quartz glass crucibles at 900°C for 60 hours. Annealed grains were transferred into 3.5 mL PFA screw top beakers, ultrapure HF (up to 50% strength, 500 mL) and HNO<sub>3</sub> (up to 14N, 50 mL) were added and caps are closed finger tight. The beakers were placed in 125 mL PTFE liners (up to four per liner) and about 2 mL HF and 0.2 mL HNO<sub>3</sub> of the same strength as acid within beakers containing samples were added to the liners. The liners were then slid into stainless steel Parr™ high pressure dissolution devices, which were sealed and brought up to a maximum of 200°C for 8-16 hours (typically 175°C for 12 hours). Beakers were removed from liners and zircon was separated from leachate. Zircons were rinsed with >18 MΩ.cm water and subboiled acetone. Then 2 mL of subboiled 6N HCl was added and beakers were set on a hotplate at 80-130°C for 30 minutes and again rinsed with water and acetone. Masses were estimated from the dimensions (volumes) of grains. Single grains were transferred into clean 300 mL PFA microcapsules (crucibles), and 50 mL 50% HF and 5 mL 14N HNO<sub>3</sub> were added. Each was spiked with a <sup>233-235</sup>U-<sup>205</sup>Pb tracer solution (EARTHTIME ET535), capped and again placed in a Parr liner (8-15 microcapsules per liner). HF and nitric acids in a 10:1 ratio, respectively, were added to the liner, which was then placed in Parr high pressure device and dissolution was achieved at 240°C for 40 hours. The resulting solutions were dried on a hotplate at 130°C, 50 mL 6N HCl was added to microcapsules and fluorides were dissolved in high pressure Parr devices for 12 hours at 210°C. HCl solutions were transferred into clean 7 mL PFA beakers and dried with 2 mL of 0.5N H<sub>3</sub>PO<sub>4</sub>. Samples were loaded onto degassed, zone-refined Re filaments in 2 mL of silicic acid emitter (Gerstenberger and Haase, 1997).

Isotopic ratios were measured by a modified single collector VG-54R or 354S (with Sector 54 electronics) thermal ionization mass spectrometer equipped with analogue Daly photomultipliers. Analytical blanks are 0.2 pg for U and up to 3 pg for Pb. U fractionation was determined directly on individual runs using the EARTHTIME ET535 mixed <sup>233-235</sup>U-<sup>205</sup>Pb isotopic tracer and Pb isotopic ratios were corrected for fractionation of 0.23%/amu, based on replicate analyses of NBS-982 reference material and the values recommended by Thirlwall (2000). Data reduction employed the Excel-based program of Schmitz and Schoene (2007). Standard concordia diagrams were constructed and regression intercepts, weighted averages calculated with Isoplot (Ludwig, 2003). Unless otherwise noted, all errors are quoted at the 2 sigma or 95% level of confidence. Isotopic dates were calculated with the decay constants  $\lambda_{238}=1.55125E-10$  and  $\lambda_{235}=9.8485E-10$  (Jaffey et al., 1971). EARTHTIME U-Pb synthetic solutions

were analysed on an on-going basis to monitor the accuracy of results.

### 3.2. LA-ICP-MS

LA-ICP-MS instrumentation included a New Wave UP-213 laser ablation system and a ThermoFinnigan Element2 single collector, double-focusing, magnetic sector ICP-MS. We used the data acquisition and reduction protocols detailed by Tafti et al. (2009), as summarized below. Zircons hand-picked from the heavy mineral concentrate were mounted in an epoxy puck along with grains of the Plešovice zircon standard (Sláma et al., 2008) and an in-house, 197 Ma standard zircon, and brought to a very high polish. High quality portions of each grain (free of alteration, inclusions, or possible inherited cores) were selected for analysis. The surface of the mount was washed for 10 minutes with dilute nitric acid and rinsed in ultraclean water before analysis. Line scans rather than spot analyses were employed to minimize elemental fractionation during the analyses. Backgrounds were measured with the laser shutter closed for ten seconds, followed by data collection with the laser firing for approximately 29 seconds. The time-integrated signals were analysed using GLITTER software (Van Aetherbergh, 2001; Griffin, 2008), which automatically subtracts background measurements, propagates all analytical errors, and calculates isotopic ratios and ages. Corrections for mass and elemental fractionation were made by bracketing analyses of unknown grains with replicate analyses of the Plešovice zircon standard. A typical analytical session consisted of four analyses of the standard zircon, followed by four analyses of unknown zircons, two standard analyses, four unknown analyses, etc., and finally four standard analyses. The 197 Ma in-house zircon standard was analysed as an unknown to monitor the reproducibility of the age determinations on a run-to-run basis. Final interpretation and plotting of the analytical results used ISOPLOT software (Ludwig, 2003). Interpreted ages are based on a weighted average of the individual calculated <sup>206</sup>Pb/<sup>238</sup>U ages. Although zircons typically contain negligible amounts of initial common Pb, it is important to monitor the amount of <sup>204</sup>Pb to evaluate the amount of initial common Pb, and/or blank Pb, in the zircons being analyzed. The argon that is used in an ICP-MS plasma commonly contains at least a small amount of Hg, and approximately 7% of natural Hg has a mass of 204. Measured count rates on mass 204 include <sup>204</sup>Hg as well as any <sup>204</sup>Pb that might be present, and direct measurement of <sup>204</sup>Pb in a laser ablation analysis is therefore not possible. Instead, mass 202 is monitored; this corresponds exclusively to <sup>202</sup>Hg. The expected count rate for <sup>204</sup>Hg present in the analysis can then be calculated from the known isotopic composition of natural Hg, and any remaining counts at mass 204 can be attributed to <sup>204</sup>Pb. Using this method, it is possible to conclude that there was no measurable <sup>204</sup>Pb present in any of the analyses in this study.

### 4. Geochronology results

One sample was submitted from the mine succession at

Granduc, and five from host rocks and adjacent strata at the Rock and Roll deposit (one did not yield sufficient zircon). Uranium-lead isotopic age determinations obtained by LA-ICP-MS are plotted in Figures 6 and 7 (tabulated and ancillary data are presented in Mihalynuk et al., 2019); those obtained by CA-TIMS are listed in Tables 2, 3 and 4.

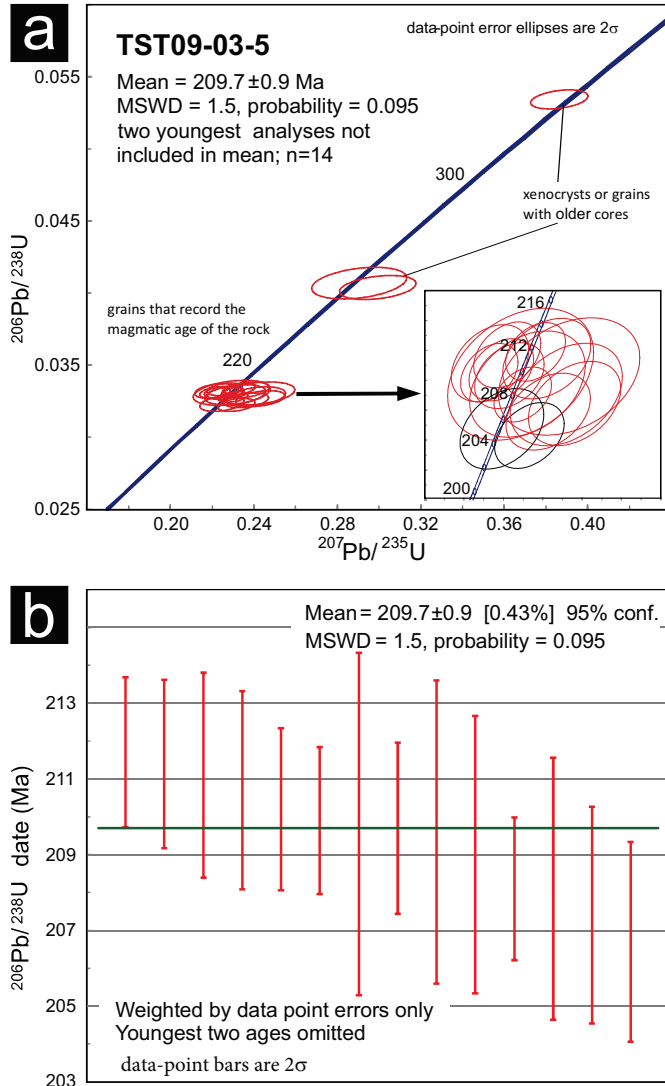


**Fig. 7. a)** Concordia plot for all zircons analyzed from sample TST09-03-5, a tuff band in deformed limestone from Rock and Roll. The inset shows details of the 14 data points used to calculate the age. **b)** Weighted mean  $^{206}\text{Pb}/^{238}\text{U}$  age of  $209.7 \pm 0.9$  Ma calculated for the cluster of zircons in the inset.

#### 4.1. Granduc

Clasts in heterolithic breccia of the mine series north and south of Leduc Glacier are primarily feldspar and lesser hornblende-feldspar porphyry. These strata have been included in the upper mine series and described as “green lapilli tuff, chert pebble conglomerate with a black calcareous matrix; minor dark green foliated volcanics” (Morrison et al., 2013, p. 68). Owing to the angularity of competent clasts in the sample analyzed, we refer to it as a breccia. The sample is a green volcanic clast-rich rock

with a fine ash-rich matrix and includes minor black argillite and light coloured, rusty-weathering pyrite and pyrrhotite-veined clasts; strained incompetent altered clasts are aligned along the fabric and appear rounded (Fig. 3a).

Sample 10JLO-10-51 was collected from a 0.6 m interval (6.3 to 6.9 m) from fresh, cut core of diamond drill hole 2006-7 (azimuth  $090^\circ$ , inclined  $-58^\circ$ , end of hole 389.9 m; McGuigan and Harrison, 2010, unpublished report cited in Morrison et al., 2013) that intersected mine series heterolithic breccia south of the Leduc Glacier (Fig. 2b). Historic drilling within this unit in the south zone intersected massive sulphide layers with true thicknesses of  $\sim 4\text{--}7$  m and grading between 3 and 4% Cu (Morrison et al., 2013).

Abundant clear, doubly terminated zircons and fragments (Fig. 6a inset) were separated from the sample. Analysis of the zircons produced a spectrum of dates with a main peak at  $\sim 208$  Ma, and a secondary peak at  $\sim 304$  Ma. Several zircons yielded ages between  $\sim 325$  and 348 Ma. The juvenile, mainly volcanic provenance of the units suggests that the  $\sim 208$  Ma age broadly represents the depositional age of the sediment. In addition, we interpret mineralized clasts in the heterolithic breccia unit as either indicating deposition that is coeval with mineralization or representing eroded or collapsed parts of an anoxic, subaqueous mineralized or mineralizing volcano-hydrothermal system. Thus, the heterolithic breccia age should broadly date VMS mineralization. The biotite and chlorite alteration displayed by the sample may be related to the same hydrothermal system or may be unrelated and due to later igneous intrusion and thermal metamorphism.

#### 4.2. Rock and Roll

##### 4.2.1. Tuff band in limestone

##### sample TST09-3-05, $209.7 \pm 0.9$ Ma

Strongly foliated and folded limestone west and northwest of Lost Lake (Fig. 2a) was previously considered to be Permian (Kerr, 1948). It contains layers packed with green lapilli and ash-sized clasts (Fig. 4a) and local resistant silty layers (Figs. 4a, b). The tuffaceous layers are typically less than 10 cm thick, although the sampled tuff layer is about 50 cm thick and pyritic, grading into pyritic carbonate. Pyrite grains within this layer display horizontal elongation in a southeast-northwest direction. Where sampled, the thick tuff layer is white and rust-weathering, possibly more felsic than other tuff layers (Fig. 4c).

Of the zircons separated from the sample, twenty grains were selected for LA-ICP-MS analysis. Fourteen of these grains define a mean  $^{206}\text{Pb}/^{238}\text{U}$  age of  $209.7 \pm 0.9$  Ma (95% confidence, Fig. 7). This age is considered to represent the crystallization age of the tuff, coeval with the surrounding limestone. This age is consistent at the stage level with late Carnian to early Norian conodont ages (Golding et al., 2017) from limestone along strike, north of the Iskut River. At the substage level, the  $\sim 210$  Ma age is younger than the conodont-bearing strata, because the early-middle Norian boundary is age calibrated at 224 Ma in British Columbia (Diakow et al., 2012) and globally (Kent et al., 2017 and citations therein). This suggests that

**Table 2. U-Th-Pb isotopic data for sample TST09-3-16.**

Compositional Parameters										Radiogenic Isotope Ratios				Isotopic Ages							
Sample	Wt.	U	Th	Pb	$^{206}\text{Pb}^*$	mol %	$\frac{\text{Pb}^*}{\text{Pb}}$	$\frac{^{206}\text{Pb}}{^{206}\text{Pb}}$	$\frac{^{207}\text{Pb}}{^{206}\text{Pb}}$	$\frac{^{208}\text{Pb}}{^{206}\text{Pb}}$	% err	$\frac{^{207}\text{Pb}}{^{235}\text{U}}$	% err	$\frac{^{206}\text{Pb}}{^{238}\text{U}}$	% err	$\frac{^{207}\text{Pb}}{^{235}\text{U}}$	% err	$\frac{^{206}\text{Pb}}{^{238}\text{U}}$	% err		
(a)	(b)	(c)	(d)	(c)	(c)	(c)	(c)	(f)	(g)	(g)	(h)	(g)	(h)	(g)	(h)	(i)	(h)	(i)	(h)	(i)	
<b>TST09-3-16</b>																					
A	0.0016	42	0.370	3.1	0.1285	85.56%	2	1.78	128	0.118	0.052288	5.493	0.333028	5.833	0.046193	0.428	0.808	298.01	125.31	291.87	14.80
B	0.0014	33	0.483	2.9	0.0908	80.55%	1	1.80	95	0.154	0.052606	7.880	0.336709	8.363	0.046421	0.593	0.828	311.84	179.30	294.68	21.39
C	0.0009	24	0.372	3.1	0.0414	65.31%	1	1.81	53	0.122	0.054434	16.990	0.349883	17.722	0.046618	1.276	0.821	389.04	374.64	304.63	46.64
D	0.0013	255	0.340	15.8	0.7750	97.06%	10	1.93	630	0.108	0.053775	0.990	0.415445	1.077	0.056031	0.164	0.584	361.64	22.33	352.79	3.21
E	0.0009	57	0.368	4.1	0.1032	87.40%	2	1.22	147	0.114	0.051342	5.266	0.338763	5.588	0.047854	0.447	0.740	256.23	121.02	296.23	14.36

(a) A, B, etc. are labels for fractions composed of single zircon grains or fragments; all fractions annealed and chemically abraded after Mattinson (2005) and Scoates and Friedman (2008).  
 (b) Nominal fraction weights estimated from photomicrographic grain dimensions, adjusted for partial dissolution during chemical abrasion.  
 (c) Nominal U and total Pb concentrations subject to uncertainty in photomicrographic estimation of weight and partial dissolution during chemical abrasion.  
 (d) Model Th/U ratio calculated from radiogenic  $^{206}\text{Pb}/^{206}\text{Pb}$  ratio and  $^{207}\text{Pb}/^{235}\text{U}$  age.  
 (e)  $\text{Pb}^*$  and  $\text{Pb}$  represent radiogenic and common Pb, respectively; mol%  $^{206}\text{Pb}^*$  with respect to radiogenic, blank and initial common Pb.  
 (f) Measured ratio corrected for spike and fractionation only. Mass discrimination of 0.23‰/amu based on analysis of NBS-982; all Daly analyses.  
 (g) Corrected for fractionation, spike, and common Pb; up to 3 pg of common Pb was assumed to be procedural blank;  $^{206}\text{Pb}/^{206}\text{Pb} = 18.50 \pm 1.0\%$ ;  $^{207}\text{Pb}/^{204}\text{Pb} = 15.50 \pm 1.0\%$ ;  $^{208}\text{Pb}/^{204}\text{Pb} = 38.40 \pm 1.0\%$  (all uncertainties 1-sigma). Excess over blank was assigned to initial common Pb with S-K model Pb composition at 291 Ma.  
 (h) Errors are 2-sigma, propagated using the algorithms of Schmitz and Schoene (2007) and Crowley et al. (2007).  
 (i) Calculations are based on the decay constants of Jaffey et al. (1971).  $^{206}\text{Pb}/^{238}\text{U}$  and  $^{207}\text{Pb}/^{206}\text{Pb}$  ages corrected for initial disequilibrium in  $^{230}\text{Th}/^{238}\text{U}$  using  $\text{Th}/\text{U}$  [magma] = 3.  
 (j) Corrected for fractionation, spike, and blank Pb only.

**Table 3. U-Th-Pb isotopic data for sample TST09-6-11.**

Compositional Parameters										Radiogenic Isotope Ratios				Isotopic Ages							
Sample	Wt.	U	Th	Pb	$^{206}\text{Pb}^*$	mol %	$\frac{\text{Pb}^*}{\text{Pb}}$	$\frac{^{206}\text{Pb}}{^{206}\text{Pb}}$	$\frac{^{207}\text{Pb}}{^{206}\text{Pb}}$	$\frac{^{208}\text{Pb}}{^{206}\text{Pb}}$	% err	$\frac{^{207}\text{Pb}}{^{235}\text{U}}$	% err	$\frac{^{206}\text{Pb}}{^{238}\text{U}}$	% err	$\frac{^{207}\text{Pb}}{^{235}\text{U}}$	% err	$\frac{^{206}\text{Pb}}{^{238}\text{U}}$	% err		
(a)	(b)	(c)	(d)	(c)	(c)	(c)	(c)	(f)	(g)	(g)	(h)	(g)	(h)	(g)	(h)	(i)	(h)	(i)	(h)	(i)	
<b>TST09-6-11</b>																					
A	0.0010	487	0.977	22.4	0.7463	97.58%	14	1.50	764	0.308	0.050505	1.774	0.256056	1.822	0.036771	0.204	0.290	218.28	41.05	231.48	3.77
B	0.0012	658	1.165	25.4	0.9620	97.19%	12	2.28	658	0.371	0.049821	1.158	0.200602	1.253	0.029203	0.262	0.451	186.63	26.96	185.64	2.13
C	0.0002	2026	1.070	93.7	0.6086	97.49%	14	1.28	736	0.338	0.050402	1.235	0.250296	1.301	0.036017	0.221	0.375	213.57	28.61	226.82	2.64

Notes as in Table 2, except as follows:  
 (g) Corrected for fractionation, spike, and common Pb; up to 3 pg of common Pb was assumed to be procedural blank;  $^{206}\text{Pb}/^{206}\text{Pb} = 18.50 \pm 1.0\%$ ;  $^{207}\text{Pb}/^{204}\text{Pb} = 15.50 \pm 1.0\%$ ;  $^{208}\text{Pb}/^{204}\text{Pb} = 38.40 \pm 1.0\%$  (all uncertainties 1-sigma). Excess over blank was assigned to initial common Pb with S-K model Pb composition at 185 Ma.

**Table 4. U-Th-Pb isotopic data for sample TST09-7-01.**

Compositional Parameters										Radiogenic Isotope Ratios				Isotopic Ages							
Sample	Wt.	U	Th	Pb	$^{206}\text{Pb}^*$	mol %	$\frac{\text{Pb}^*}{\text{Pb}}$	$\frac{^{206}\text{Pb}}{^{206}\text{Pb}}$	$\frac{^{207}\text{Pb}}{^{206}\text{Pb}}$	$\frac{^{208}\text{Pb}}{^{206}\text{Pb}}$	% err	$\frac{^{207}\text{Pb}}{^{235}\text{U}}$	% err	$\frac{^{206}\text{Pb}}{^{238}\text{U}}$	% err	$\frac{^{207}\text{Pb}}{^{235}\text{U}}$	% err	$\frac{^{206}\text{Pb}}{^{238}\text{U}}$	% err		
(a)	(b)	(c)	(d)	(c)	(c)	(c)	(c)	(f)	(g)	(g)	(h)	(g)	(h)	(g)	(h)	(i)	(h)	(i)	(h)	(i)	
<b>TST09-7-01</b>																					
A	0.0067	100	0.415	3.5	0.7995	94.16%	5	4.08	317	0.132	0.049804	1.902	0.197524	2.047	0.028764	0.337	0.498	185.86	44.27	183.03	3.43
B	0.0067	174	0.467	5.3	1.3967	99.13%	34	1.00	2134	0.149	0.050031	0.570	0.198494	0.648	0.028775	0.180	0.545	196.42	13.24	183.85	1.09
C	0.0081	103	0.620	3.4	1.0191	98.07%	16	1.65	956	0.197	0.049800	1.622	0.200778	1.747	0.029241	0.269	0.527	185.66	37.75	185.78	2.97
D	0.0084	181	0.406	5.4	1.8269	99.26%	40	1.11	2504	0.129	0.049582	0.482	0.197267	0.597	0.028856	0.300	0.599	175.45	11.24	182.81	1.00
E	0.0020	366	0.570	12.0	0.8774	97.66%	13	1.73	791	0.180	0.049258	1.235	0.195337	1.338	0.028762	0.229	0.520	160.11	28.88	181.17	2.22

Notes as in Table 2, except as follows:  
 (g) Corrected for fractionation, spike, and common Pb; up to 3 pg of common Pb was assumed to be procedural blank;  $^{206}\text{Pb}/^{206}\text{Pb} = 18.50 \pm 1.0\%$ ;  $^{207}\text{Pb}/^{204}\text{Pb} = 15.50 \pm 1.0\%$ ;  $^{208}\text{Pb}/^{204}\text{Pb} = 38.40 \pm 1.0\%$  (all uncertainties 1-sigma). Excess over blank was assigned to initial common Pb with S-K model Pb composition at 183 Ma.

limestone at Lost Lake was deposited over a protracted (>10 m.y.) period.

#### 4.2.2. Cherty siltstone sample TST09-3-16, 291.7 ±1.0 Ma

Laminated, cream to rusty weathering, cherty, tuffaceous siltstone with a structural thickness of up to 100 m occurs to the north and east of Lost Lake (Fig. 2a). This tuffaceous siltstone (Fig. 8a) appears to grade to the southeast into felsic lapilli tuff. Other parts of the unit include cherty layers within fine siltstone, and argillite with siliceous ovoids interpreted as recrystallized radiolaria (Fig. 8b). We collected a sample from an outcrop of suspected rhyolitic dust tuff (near outcrop of Fig. 8a) to test for age equivalence with other tuffaceous layers, but petrographic analysis revealed little definitive evidence of volcanic textures.

Of the zircons separated from the sample, five were selected for CA-TIMS analysis. Three concordant and overlapping  $^{206}\text{Pb}/^{238}\text{U}$  dates produced a weighted average age of 291.7 ±1.0 Ma; two older concordant analyses are interpreted as recording older sources or xenocrystic cores (Fig. 9). The 291.7 ±1.0 Ma age is interpreted as the crystallization age of the predominant source of the tuffaceous siltstone. This age is ~80 m.y. older than the other ages reported here and thus

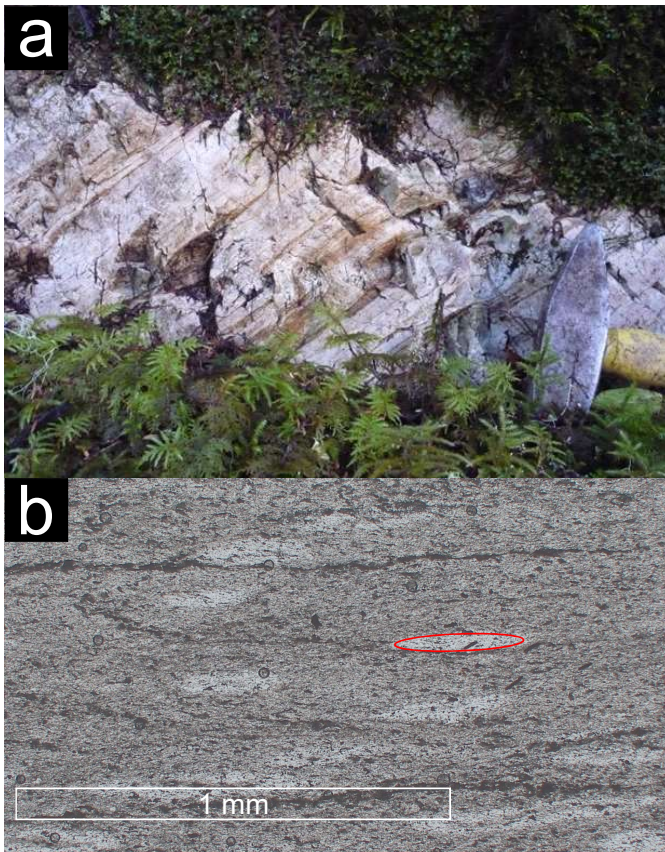


**Fig. 8.** a) Representative outcrop of cherty, tuffaceous siltstone at Rock and Roll like that sampled for age determination (Sample TST09-3-16). b) Plane polarized light photomicrograph of cherty and silty argillite sample. Clear ovoids (one highlighted by red oval) are interpreted as recrystallized radiolaria.

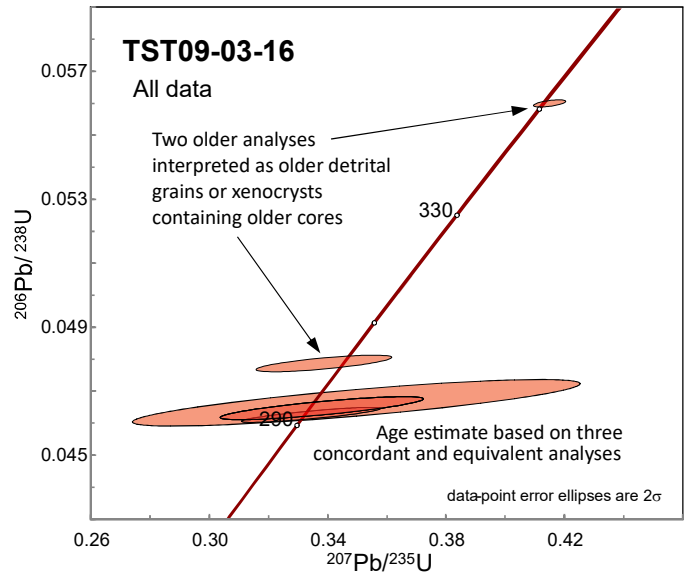


**Fig. 9.** Concordia plot of five grains analyzed by CA-TIMS from sample TST09-3-16. An age of the sample of 291.7 ±1.0 Ma is interpreted based on three overlapping and equivalent dates.

its significance is unclear. One possibility is that the sample is from a Triassic sequence that was predominantly derived from an Early Permian and older basement with  $^{206}\text{Pb}/^{238}\text{U}$  ages of 301 ±1 Ma and 351.4 ±0.6 Ma, such as igneous basement identified regionally by, for example, Logan et al. (2000). We consider this unlikely because it would require the depocentre be shielded somehow from sediments shed from the active Stuhini arc, which are amply represented by zircon-bearing Triassic volcanic and plutonic rocks regionally. An alternative and more likely explanation is that this rock is part of the Stikine assemblage (Paleozoic) and that there is either an unconformity or an unrecognized fault in this area.

#### 4.2.3. Diorite sample TST09-6-11, 185.6 ±0.5 Ma

Variably foliated, dark green and light grey-weathering diorite sills and dikes up to 50 m thick cut all lithologies around Lost Lake and form resistant rounded to blocky outcrops (Fig. 5a). Dikes are predominantly parallel and perpendicular to northwest-trending folds (Fig. 2a). A sample of medium-grained, hornblende-feldspar-titanite quartz diorite (~5% interstitial quartz) was sampled near the main Black Dog showing at the Rock and Roll property for CA-TIMS dating. The sample yielded very few zircons, and only three grains survived chemical abrasion pre-treatment intact. TIMS analysis of these grains produced a maximum age based on  $^{206}\text{Pb}/^{238}\text{U}$  date of the youngest grain of 185.6 ±0.5 Ma (Fig. 10). This age is interpreted as the crystallization age of the quartz diorite, and because these dikes cut sulphide mineralization at the Black Dog occurrence (Fig. 2a), it provides an absolute minimum age for the mineralization.

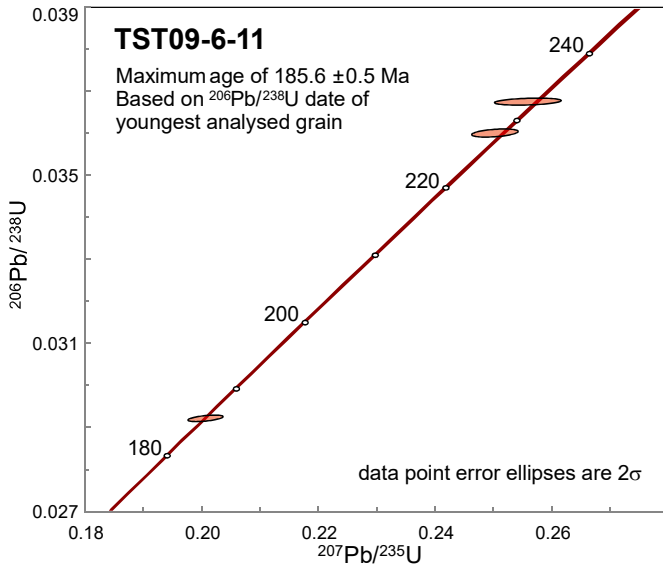


**Fig. 10.** Concordia plot of three grains analyzed by CA-TIMS from sample TST09-6-11. A maximum age of the sample of  $185.6 \pm 0.5$  Ma is interpreted based on the youngest grain.

#### 4.2.4. Rhyodacitic dike

##### sample TST09-7-01, $182.92 \pm 0.22$ Ma

Diamond drill hole RR91-70 (Fig. 2a) north of Lost Lake intersected an interval of felsic rock within the laminated volcanic siltstone unit. Split core was retrieved from a 7 m interval (5.2-12.2 m) for dating. Petrographic analysis of a subsample shows preservation of delicate trachytic fabric with no sign of the penetrative foliation seen in all other samples (Fig. 11). The petrography and lack of foliation suggests that the felsic rock is likely a dike that cuts the laminated volcanic siltstone. Of the zircons separated from the sample, four grains were analysed by CA-TIMS producing concordant and overlapping dates with a  $^{206}\text{Pb}/^{238}\text{U}$  weighted age of  $182.92 \pm 0.22$  Ma (Fig. 12). We interpret this as the crystallization age of a dike that postdates deformation. A slightly older  $\sim 186$  Ma grain is interpreted as a xenocryst or a grain containing an older core, perhaps derived from one of the widespread diorite dikes of this age.

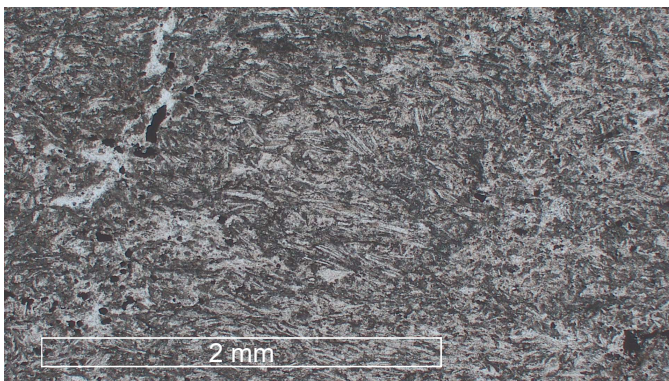


**Fig. 11.** Fine trachytic texture preserved in sample TST09-7-01 is outlined by feldspar microlites.

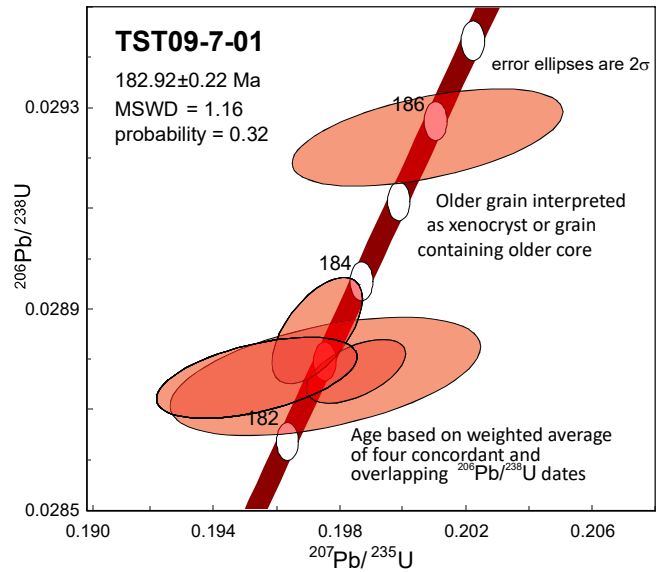


**Fig. 12.** Concordia plot of five grains analyzed by CA-TIMS from sample TST09-7-01. A relatively precise age of the sample of  $182.92 \pm 0.22$  Ma is interpreted based on four overlapping and equivalent dates.

#### 4.2.5. Rhyolite tuff and pyritic rhyolite tuff sample TST09-3-02, no age determination

Laminated, black to green-grey and rust to black weathering silty mudstone contains 1-1.5 cm thick, cream coloured quartz and feldspar-rich layers interpreted as volcanic tuff. In places the feldspar is altered and deformed around quartz eyes, which are up to 3 mm in diameter. However, petrographic analysis of these layers show that they contain a few percent by volume microperthite grains (Fig. 13), indicating a slowly cooled, not eruptive, igneous source. Repetition of laminated and graded layers within the silty mudstone are interpreted to record subaqueous mass flows. A sample of the tuff did not contain sufficient zircon for age determination.

## 5. Discussion

Ages obtained in this study help to constrain the timing of mineralization at Granduc and Rock and Roll. Our data indicate that the mineralization at Granduc may be younger than  $\sim 222$  Ma (Childe, 1997), with its younger age limit approximately dated by the youngest zircon population,  $\sim 208$  Ma, in the heterolithic breccia of the 'Mine Series'. Preservation of sulphide clasts suggests that deposition of breccia was either coeval with or shortly postdated the upper mineralized horizon at Granduc. Heterolithic breccias are common features of hydrothermal fields because the sub-basins in which they occur are bounded by active fault scarps that produce talus. In addition, hydrothermal mounds grow, over-steepen and collapse. Ancient and modern examples of heterolithic breccias are known worldwide: Canada, Peru, Turkey, Japan, Australia, Russia, TAG, PACMANUS, Middle Valley (Whalen et al., 2013; Tornos et al., 2015). Heterolithic breccia in many of these deposits are mixtures of volcanic, argillite, and sulphide clasts, lithologically similar to the heterolithic mine stratigraphy unit

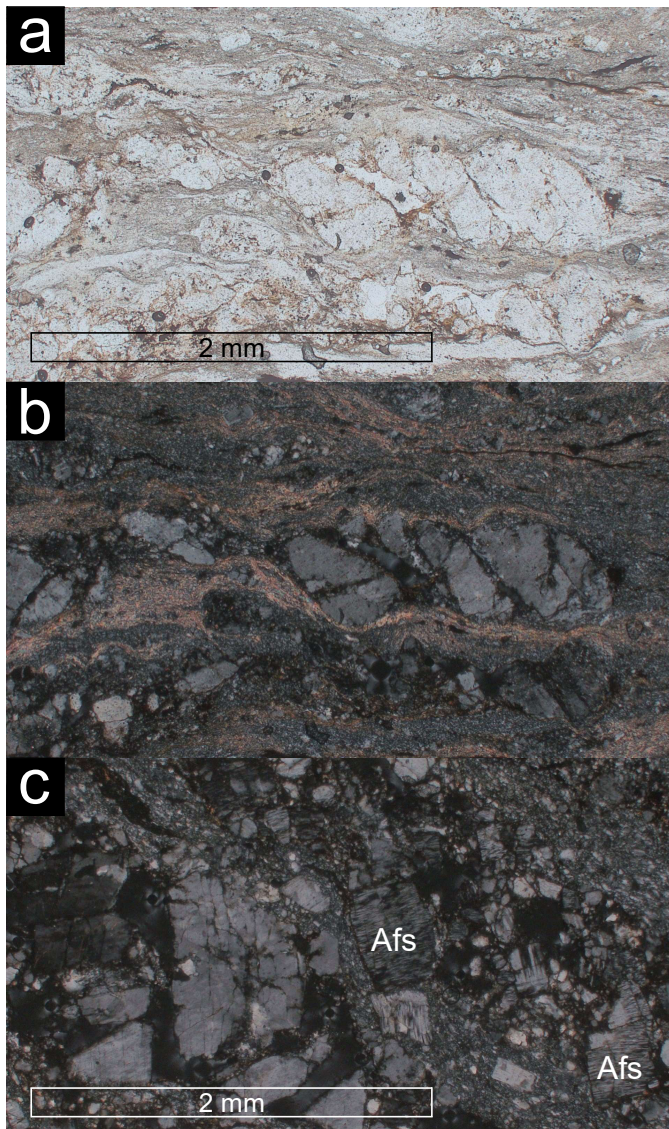


**Fig. 13.** Photomicrographs of coarse ‘ash tuff’ layer, a subsample of TST09-3-02. **a)** Plane polarized light showing cataclastic reduction of feldspar crystals and a well-developed shear fabric. **b)** Same view in cross polarized light. **c)** Another view of the same thin section showing abundant micropertthite grains (Afs: alkali feldspar) of probable intrusive origin.

at Granduc, which is strikingly similar to heterolithic breccia immediately overlying massive sulphide mineralization at the Rock and Roll (Fig. 3). Such similarity suggest that these deposits accumulated in basins with analogous flanking strata and modes of deposition.

At Rock and Roll, the oldest dated strata are ~292 Ma (Early Permian, Sakmarian; Cohen et al., 2013, updated 2018). Extensive carbonate rocks, previously presumed to be part of the Stikine assemblage (Permian), has now been confirmed as containing a ~210 Ma tuff layer (Fig. 7) and are therefore Late Triassic (Late Norian). This age is broadly consistent with conodont ages on correlative limestone within the Stuhini Group north of the Iskut River (Golding et al., 2017). The

Norian age of the limestone negates the need for an interpreted southwest-dipping thrust fault at its base (e.g., as shown by Mihalynuk et al., 2010). It is likely that the immediate host strata of the Rock and Roll deposit lie stratigraphically between the Norian limestone unit and the Permian siltstone, with an age of between 210 Ma and 292 Ma. Although these age constraints are broad, they are consistent with the 222 to 208 Ma age of the Granduc deposit.

Lead isotopic signatures also support their correlation. The  $^{207}\text{Pb}/^{204}\text{Pb}$  cluster from galena and pyrite mineralization at Granduc and galena at the Rock and Roll deposit are identical within error (Dean and Carr, 1991; Childe, 1997). Late Triassic model ages for Granduc and Rock and Roll coincide with those for Greens Creek VMS deposit (Alexander terrane) and the Schaft Creek porphyry copper deposit (Stikine terrane), both of which have independently dated Late Triassic hosts (Childe, 1997; Logan et al., 2000; Sack, 2009; Sack et al., 2016; Taylor et al., 2010). Overlap of lead  $^{208}\text{Pb}/^{204}\text{Pb}$  clusters for Tulsequah and Granduc remains problematic. It may reveal some resetting of that isotopic system at Tulsequah, and requires re-evaluation.

Ages of minor pre-Triassic zircon populations in our samples help to further resolve the discontinuously exposed Paleozoic Stikine assemblage basement of northern Stikinia. Inherited and detrital zircons from Rock and Roll (~301 and 351 Ma) and Granduc (~304, 325 and 348 Ma) indicate that Stikine assemblage was present as adjacent highlands or basement to these sequences, suggesting that it extends beneath younger cover.

### 5.1. Late Triassic mineralization in Stikinia

Late Triassic Stikine and Quesnel terranes are mostly known for their Cu-Au ±Ag-Pt-Pd-Mo porphyry and related mineralization (Logan and Mihalynuk, 2014). Porphyry mineralization is known to be spatially associated with volcano-plutonic complexes. However, mineral deposit studies typically underappreciate that volcanic rocks were in many cases deposited in marine environments, as indicated by intercalated volcanic and marine sedimentary rocks, some bearing coeval marine fossils. Marine environments coeval and co-spatial with porphyry mineralization are commonly recorded by Mesozoic Stikinia and Quesnellia rocks. Arc-proximal, fault-bounded, restricted basins with slow sedimentation (e.g., containing carbonaceous argillite), and signs of hydrothermal alteration or exhalites, have significant potential for accumulations of VMS mineralization.

Although we now have a geochronological framework that is consistent with a Late Triassic age of massive sulphide mineralization at both Granduc and Rock and Roll deposits, the absolute age of mineralization has still not been determined. Units unequivocally contemporaneous with sulphide mineralization need to be dated, or the sulphide mineralization needs to be directly dated. Determining the age of sulphide mineralization may be possible using the Re-Os technique if sulphide minerals such as pyrrhotite, pyrite, sphalerite, chalcopyrite, galena at Rock and Roll contain sufficient radiogenic Re. Unfortunately,

unlike graphitic shales elsewhere (Selby and Creaser, 2005), the two samples of Rock and Roll sulphide mineralization in graphitic shale at the Black Dog occurrence lacked sufficient rhenium for a direct Re/Os age determination. Because Re is concentrated in molybdenite, any trace of this mineral found in the VMS mineralization at either deposit should be collected for Re-Os age determination.

## 5.2. Early Jurassic magmatism and age constraints on deformation

Late syn- to post-kinematic ~186 Ma quartz diorite dikes at Rock and Roll are only locally foliated, but display pervasive mesoscopic brittle deformation and grain size reduction (Fig. 5), whereas the ~183 Ma felsic trachytic dike (drill core sample TST09-7-01) is undeformed (Fig. 11). The 186 Ma grain in the analyzed ~183 Ma dike sample, likely inherited when crosscutting the older quartz diorite dikes, is consistent with the relative age assignments of these intrusions.

The ages of the Rock and Roll dikes are coeval with younger part of the Texas Creek Plutonic suite (ca. 195-178 Ma; Lewis 2013) and are coeval with the most prolific Early Jurassic magmatic suite in the northern Cordillera, the Aishihik suite (*sensu* Johnston et al., 1996; Mihalynuk et al., 1999). The Texas Creek Plutonic suite includes plutons, stocks, and dikes that are widespread in the Iskut River area, and are considered to have fed extrusive magmatic rocks of the Betty Creek Formation (Lewis, 2013; Cutts et al., 2015). A nearby coeval, possible extrusive equivalent of the Rock and Roll diorite (sample TST09-6-11) in the Hoodoo Mountain area is a grey, hornblende (5-10%) and plagioclase (35-40%) porphyritic ash flow that returned 187.0 ± 1.9 Ma zircons (MMI10-13-2; Mihalynuk et al., 2011). Zircons from the ash flow also contain ~560 and 1800 Ma inheritance (Zagorevski et al., 2015) not yet identified in the diorite dikes at Rock and Roll.

The ~183 Ma felsic trachytic dike (drill core sample TST09-7-01) is roughly coeval with tuffaceous sandstones near Hoodoo Mountain. There, a carbonate-cemented quartzite and pebble conglomerate cut by gabbro sills returned a unimodal detrital zircon population at 181.8 ± 1.7 Ma (N. Joyce, unpublished results from sample ZE10-294A) and 184.3 ± 2.2 Ma (N. Joyce, unpublished results from sample 14ZE842B).

Two deformation events fold and foliate rocks that we now know to be Late Triassic (Figs. 3, 4, 8, 13). Clear evidence of non-coaxial overprinting of an earlier foliation by a later foliation is common (Fig. 4). Late Early Jurassic bodies provide younger age constraints on the second penetrative deformation that affected Stuhini Group and older strata, ending in the lower Iskut River area between 186 and 183 Ma. The older of these two deformational events is amply represented along the Intermontane belt (Fig. 1) in late Norian to early Rhaetian, and is implicated in the formation of porphyry copper deposits (Logan and Mihalynuk, 2014). The younger event may be related to crustal thickening in northern Stikinia and at peak metamorphic pressures ~185 Ma (Mihalynuk et al., 1999). At the same time, widespread zircon lead loss (Mihalynuk et

al., 2006) and contraction (Nixon et al., 1993) are recorded along the inboard margin of the northern Intermontane belt. Younger deformational episodes are not recorded by rocks at Rock and Roll. For example, they show little evidence of either the Middle Jurassic contraction affecting the entire northeast margin of Stikinia and which inverted the Whitehorse trough (Mihalynuk et al., 2004; Mihalynuk et al., 2017), nor of mid-Cretaceous shortening in adjacent Bowser Basin, manifested by the Skeena fold and thrust belt (Evenchick et al., 2007).

## 6. Summary

This study provides new age constraints on the Granduc past-producer and the Rock and Roll deposit. Host rocks of both are Upper Triassic and assigned to the Stuhini Group. A new detrital maximum depositional age for host strata in the 'Mine Series' at Granduc is ~208 Ma, distinctly younger than ~222 Ma U-Pb ages from igneous protoliths reported by Childe (1997). Host rocks at Rock and Roll formed between 292 and 210 Ma. Similarity of mineralization and of local deposit stratigraphy favours consideration of these two deposits as products of a VMS epoch within the Stuhini Group that may have regional potential.

## Acknowledgments

Samples were collected by Toby Stiers, University of Victoria. LA-ICP-MS analyses were by Kathryn Lucas, PCIGR, Department of Earth and Ocean Sciences, The University of British Columbia. Sample collection and geochronology was supported by a NSERC Discovery Grant to S.T. Johnston. Reviews by H. Awmack and J. Nelson significantly improved the manuscript.

## References cited

- Childe, F., 1996. U-Pb geochronology and Nd and Pb isotope characteristics of the Au-Ag-rich Eskay Creek volcanogenic massive sulphide deposit, British Columbia. *Economic Geology* 91, 1209-1224.
- Childe, F., 1997. Timing and tectonic setting of volcanogenic massive sulphide deposits in British Columbia: constraints from U-Pb geochronology, radiogenic isotopes, and geochemistry. Unpublished Ph.D. thesis, The University of British Columbia, 319 p.
- Cohen, K.M., Finney, S.C., Gibbard, P.L., and Fan, J.X., 2013. The ICS International Chronostratigraphic Chart. *Episodes*, 36, 199-204.
- Cutts, J.A., McNicoll, V.J., Zagorevski, A., Anderson, R.G., and Martin, K., 2015. U-Pb geochronology of the Hazelton Group in the McTagg anticlinorium, Iskut River area, northwestern British Columbia. In: *Geological Fieldwork 2014*, British Columbia Ministry of Energy and Mines, British Columbia Geological Survey Paper 2015-1, pp. 87-101.
- Dean, J.A., and Carr, G.R., 1991. Report to Prime Exploration on the lead isotopic compositions of samples from Galore Creek and Iskut River, British Columbia, Unpublished Report SR 154, CSIRO Australia, 16 p.
- Diakow, L.J., Orchard, M.J., and Friedman, R.M., 2012. Absolute ages for the Norian Stage: a further contribution from southern British Columbia, Canada. *Cordilleran Tectonics Workshop*, Geological Association Canada, Pacific Section, p. 2.
- Evenchick, C.A., McMechan, M.E., McNicoll, V.J., and Carr, S.D.,

2007. A synthesis of the Jurassic-Cretaceous tectonic evolution of the central and southeastern Canadian Cordillera: Exploring links across the orogen. In: Sears, J.W., Harms, T.A., and Evenchick, C.A. (Eds.), *Whence the Mountains? Inquiries into the Evolution of Orogenic Systems: A Volume in Honor of Raymond A. Price*, Geological Society of America Special Paper, 433, pp. 117-145.
- Gagnon, J.F., Barresi, T., Waldron, J.W.F., Nelson, J.L., Poulton, T.P., and Cordey, F., 2012. Stratigraphy of the upper Hazelton Group and Jurassic evolution of the Stikine terrane, British Columbia. *Canadian Journal of Earth Sciences*, 49, 1027-1052.
- Galley, A.G., Hannington, M.D., and Jonasson, I.R., 2007. Volcanogenic massive sulphide deposits. In: Goodfellow, W.D., (Ed.), *Mineral deposits of Canada: A synthesis of major deposit-types, district metallogeny, the evolution of geological provinces, and exploration methods*. Geological Association of Canada, Mineral Deposits Division, Special Publication, 5, pp. 141-161.
- Gerstenberger, H., and Haase, G., 1997. A highly effective emitter substance for mass spectrometric Pb isotope ratio determinations. *Chemical Geology*, 136, 309-312.
- Golding, M., Orchard, M.J., and Zagorevski, A., 2017. Conodonts from the Stikine Terrane in northern British Columbia and southern Yukon. Geological Survey of Canada. Open File 8278, 23 p.
- Griffin, W.L., Powell, W.J., Pearson, N.J., and O'Reilly, S.Y., 2008. Glitter: Data reduction software for laser ablation ICP-MS. In: Sylvester, P.J. (Ed.), *Laser Ablation ICP-MS in the Earth Sciences: Current Practices and Outstanding Issues*. Mineralogical Association of Canada Short Course 40, Vancouver, B.C., pp. 308-311.
- Höy, T., 1991. Volcanogenic massive sulphide deposits in British Columbia. In: McMillan, W.J. (Ed.), *Ore Deposits, Tectonics and Metallogeny in the Canadian Cordillera*. British Columbia Ministry of Energy, Mines and Petroleum Resources, British Columbia Geological Survey Paper 1991-4, pp. 89-124.
- Jaffey, A.H., Flynn, K.F., Glendenin, L.E., Bentley, W. T., and Essling, A.M., 1971. Precision measurement of half-lives and specific activities of U 235 and U 238. *Physical Review C*, 4, 1889-1906.
- Johnston, S.T., Mortensens, J.K., and Erdmer, P., 1996. Igneous and metaigneous age constraints for the Aishihik metamorphic suite, southwest Yukon. *Canadian Journal of Earth Sciences*, 33, 1543-1555.
- Jones, M., 2011. 2010 Geological and geochemical report on the Rock and Roll Property. Assessment Report AR32127, B.C. Ministry of Energy and Mines, 58 p.
- Kent, D.V., Olsen, P.E., and Muttoni, G., 2017. Astrochronostratigraphic polarity time scale (APTS) for the Late Triassic and Early Jurassic from continental sediments and correlation with standard marine stages. *Earth Science Reviews*, 166, 153-180.
- Kerr, F.A., 1948. Lower Stikine and Iskut River areas, British Columbia. Geological Survey of Canada, Memoir 246, 94 p.
- Kyba, J., and Nelson, J., 2015. Stratigraphic and tectonic framework of the Khyber-Sericite-Pins mineralized trend, lower Iskut River, northwest British Columbia. In: *Geological Fieldwork 2014*, British Columbia Ministry of Energy and Mines, British Columbia Geological Survey Paper 2015-1, pp. 41-58.
- Lewis, P.D., 2013. Iskut River Area Geology, Northwest British Columbia (104B/08, 09, 10 & part of 104B/01, 07, 11). *Geoscience British Columbia Report 2013-05*, 1:50,000 scale.
- Logan, J.M., and Mihalynuk, M.G., 2014. Tectonic controls on early Mesozoic paired alkaline porphyry deposit belts (Cu-Au ±Ag-Pt-Pd-Mo) within the Canadian Cordillera. *Economic Geology*, 109, 827-858.
- Logan, J.M., Drobe, J.R., and McClelland, W.C., 2000. Geology of the Forrest Kerr-Mess Creek Area. Northwest British Columbia (NTS 104B/10, 15 & 104G/2 & 7W). British Columbia Ministry of Energy and Mines, British Columbia Geological Survey Bulletin, 104, 164 p.
- Ludwig, K.R., 2003. *Isoplot 3.09-A geochronological toolkit for Microsoft Excel*: Berkeley Geochronology Center, Special Publication No. 4.
- Mattinson, J.M., 2005. Zircon U-Pb chemical abrasion ("CA-TIMS") method: combined annealing and multi-step partial dissolution analysis for improved precision and accuracy of zircon ages. *Chemical Geology*, 220, 47-66.
- McGuigan, P.J., 2005. Granduc property northwestern British Columbia, Canada. Unpublished report by Tecucomp Geological Inc. for Bell Resources Corporation, 52 p.
- Mihalynuk, M.G., Mountjoy, K.J., Smith, M.T., Currie, L.D., Gabites, J.E., Tipper, H.W., Orchard, M.J., Poulton, T., P., and Cordey, F., 1999. Geology and mineral resources of the Tagish Lake area (NTS 104M/8, 9, 10E, 15 and 104N/12W), northwestern British Columbia. British Columbia Ministry of Energy, Mines and Petroleum Resources, British Columbia Geological Survey Bulletin 105, 235 p.
- Mihalynuk, M.G., Erdmer, P., Ghent, E.D., Cordey, F., Archibald, D.A., Friedman, R.M., and Johannson, G.G., 2004. Coherent French Range blueschist: Subduction to exhumation in <2.5 my? *Geological Society of America Bulletin*, 116, 910-922.
- Mihalynuk, M.G., Friedman, R.M., Devine, F.A., and Heaman, L.M., 2006. Protolith age and deformation history of the Big Salmon Complex, relics of a Paleozoic continental arc in northern British Columbia. In: Colpron, M. and Nelson, J.L. (Eds.), *Paleozoic Evolution and Metallogeny of Pericratonic Terranes at the Ancient Pacific Margin of North America, Canadian and Alaska Cordillera*. Geological Association of Canada Special Paper, 45, 179-200.
- Mihalynuk, M.G., Stier, Toby J., Jones, Murray I., R.M., and Johnston, S.T., 2010. Stratigraphic and Structural Setting of the Rock and Roll Deposit, Northwest British Columbia (NTS 104B/11). In: *Geological Fieldwork 2009*, British Columbia Ministry of Forests, Mines and Lands, British Columbia Geological Survey Paper 2010-1, pp. 7-18.
- Mihalynuk, M.G., Logan, J.M., and Zagorevski, A., 2011. East Hoodoo Mountain - Iskut River Geology, NTS 104B/14E & 11NE. Geological Survey of Canada, Open File 6730; British Columbia Ministry of Energy and Mines, British Columbia Geological Survey Open File Map, 2011-4, 1:50,000 scale.
- Mihalynuk, M.G., Zagorevski, A., English, J.M., Orchard, M.J., Bidgood, A.K., Joyce, N., and Friedman, R.M., 2017. Geology of the Sinwa Creek area, northwest BC (104K/14). In: *Geological Fieldwork 2016*, British Columbia Ministry of Energy and Mines, British Columbia Geological Survey Paper 2017-1, pp. 153-178.
- Mihalynuk, M.G., Friedman, R.M., and Logan, J.M., 2019. Detrital zircon geochronological data from the Granduc and Rock and Roll deposits, northwest British Columbia. British Columbia Ministry of Energy, Mines and Petroleum Resources, British Columbia Geological Survey GeoFile, in press.
- Montgomery, A.T., Todoruk, S.L., and Ikona, C.K., 1991. Eurus Resources Corp. Thios Resource Inc. Assessment Report on the Rock and Roll Project. British Columbia Ministry of Energy, Mines and Petroleum Resources, Assessment Report 20884, 203 p. plus figures, appendices and maps.
- Morrison, R., McKinnon, C., Liukko, G., Kesavanathan, D., Gagnon, A., Abdel Hafez, S., Danon-Schaffer, M., McLaughlin, M., and Ouellet, J., 2013. Preliminary economic assessment of the Granduc copper project, northern British Columbia. NI 43-101, Report by Tetra Tech for Castle Resources, Toronto, ON, Canada, 299 p.
- Mundil, R., Ludwig, K.R., Metcalfe, I., and Renne, P.R., 2004. Age and timing of the Permian mass extinctions: U/Pb dating of closed-system zircons. *Science*, 305, 1760-1763.
- Nixon, G.T., Archibald, D.A., and Heaman, L.M., 1993. <sup>40</sup>Ar-<sup>39</sup>Ar and U-Pb geochronometry of the Polaris alaskan-type complex, British Columbia; precise timing of Quesnellia-North America

- interaction. In: Geological Association of Canada, Mineralogical Association of Canada, Canadian Geophysical Union Joint Annual Meeting, Program With Abstracts, p. 76.
- Rhys, D.A., 1995. The Red Bluff gold-copper porphyry and associated precious and base metal veins, northwestern British Columbia. In: Schroeter, T.G. (Ed.), *Porphyry Deposits of the Northwestern Cordillera of North America*. Canadian Institute of Mining and Metallurgy Special Volume 46, pp. 838-850.
- Sack, P.J., 2009. Characterization of footwall lithologies to the Greens Creek volcanic-hosted massive sulfide (VHMS) deposit, Alaska, USA. Unpublished Ph.D. thesis, University of Tasmania, Hobart, Australia, 415 p.
- Sack, P.J., Berry, R.F., Gemmill, J.B., Meffre, S., and West, A., 2016. U-Pb zircon geochronology from the Alexander terrane, southeast Alaska: implications for the Greens Creek massive sulphide deposit. *Canadian Journal of Earth Sciences*, 53, 1458-1475.
- Schmitz, M.D., and Schoene, B., 2007. Derivation of isotope ratios, errors, and error correlations for U-Pb geochronology using  $^{205}\text{Pb}$ - $^{235}\text{U}$ -( $^{233}\text{U}$ )-spiked isotope dilution thermal ionization mass spectrometric data. *Geochemistry, Geophysics, Geosystems*, 8, 20 p.
- Scoates, J.S., and Friedman, R.M., 2008. Precise age of the platiniferous Merensky Reef, Bushveld Complex, South Africa, by the U-Pb zircon chemical abrasion ID-TIMS technique. *Economic Geology*, 103, 465-471.
- Selby, D., and Creaser, R.A., 2005. Direct radiometric dating of the Devonian-Mississippian time-scale boundary using the Re-Os black shale geochronometer. *Geology*, 33, 545-548.
- Sláma, J., Košler, J., Condon, D.J., Crowley, J.L., Gerdes, A., Hanchar, J.M., Horstwood, M.S., Morris, G.A., Nasdala, L., and Norberg, N., 2008. Plešovice zircon-a new natural reference material for U-Pb and Hf isotopic microanalysis. *Chemical Geology*, 249, 1-35.
- Tafti, R., Mortensen, J.K., Lang, J.R., Rebagliati, M., and Oliver, J.L., 2009. Jurassic U-Pb and Re-Os ages for the newly discovered Xietongmen Cu-Au porphyry district, Tibet, PRC: Implications for metallogenic epochs in the southern Gangdese belt. *Economic Geology*, 104, 127-136.
- Taylor, C.D., Premo, W.R., and Johnson, C.A., 2010. Sulfur and Lead Isotope characteristics of the Greens Creek polymetallic massive sulfide deposit, Admiralty Island, southeastern Alaska. In: Taylor, C.D., and Johnson, C.A. (Eds.), *Geology, Geochemistry, and Genesis of the Greens Creek Massive Sulfide deposit, Admiralty Island, southeastern Alaska*. U.S. Geological Survey Professional Paper 1763, pp. 241-282.
- Thirlwall, M.F., 2000. Inter-laboratory and other errors in Pb isotope analyses investigated using a  $^{207}\text{Pb}$ - $^{204}\text{Pb}$  double spike. *Chemical Geology*, 163, 299-322.
- Tornos, F., Peter, J.M., Allen, R., and Conde, C., 2015. Controls on the siting and style of volcanogenic massive sulphide deposits. *Ore Geology Reviews*, 68, 142-163.
- Van Achterbergh, E., Ryan, C.G., Jackson, S.E., and Griffin, W.L., 2001. Data reduction software for LA-ICP-MS: appendix. In: Sylvester, P.J. (Ed.), *Laser Ablation-ICP Mass Spectrometry in the Earth Sciences: Principles and Applications*. Mineralogical Association of Canada Short Course 29, Ottawa, Ontario, pp. 239-243.
- Whalen, J.B., Zagorevski, A., McNicoll, V.J., and Rogers, N., 2013. Geochemistry, U-Pb geochronology, and genesis of granitoid clasts in transported volcanogenic massive sulfide ore deposits, Buchans, Newfoundland. *Canadian Journal of Earth Sciences*, 50, 1116-1133.
- Wheeler, J.O., Brookfield, A.J., Gabrielse, H., Monger, J.W.H., Tipper, H.W., and Woodsworth, G.J., 1991. Terrane map of the Canadian Cordillera. Geological Survey of Canada, Map 1713A, 1:2,000,000 scale.
- Zagorevski, A., Mihalynuk, M.G., Joyce, N., Friedman, R.M., Ryan, J.J., Chapman, J., Cutts, J.A., McNicoll, V.J., and Anderson, R.G., 2015. Geochronology of the Lower Jurassic Hazelton arc in northwestern British Columbia and Yukon. Mineral Exploration Roundup, Poster, Association for Mineral Exploration, Vancouver, BC.